PAPER

Check for updates

Influence of Mn on the iron-based friction material directly prepared by *in situ* carbothermic reaction from vanadium-bearing titanomagnetite concentrates

Yue Shui, [ID] Keqin Feng,* Yanyan Zhang and Zidi Yan

In this work, we prepared an iron-based frictional material from vanadium-bearing titanomagnetite concentrates by *in situ* carbothermic reaction with improved tribological properties. Effects of Mn content (1–4 wt%) on the microstructure and properties of iron-based friction material were investigated. The microstructure and properties of iron-based friction material with Mn are significantly improved. In particular, the friction coefficient decreases from 0.54 to 0.40–0.49 and the wear rate reduces from 1.899×10^{-7} cm^3 J^{-1} to 0.229×10^{-7} cm^3 J^{-1} – 1.309×10^{-7} cm^3 J^{-1}. Appropriate Mn addition (1–3 wt%) contributes efficiently to the sintering densification and increasing laminated pearlites. Comparatively, the density, hardness and wear resistance are improved. The dominant wear mechanism changes from severe abrasive wear to mild abrasive wear and oxidative wear is also enhanced. However, when Mn content increases to 4 wt%, the microstructure, relative density, hardness and wear performance of iron-based friction material are deteriorated. Consequently, the optimal addition of Mn is 3 wt% in the iron-based friction material.

1. Introduction

In the Panxi area of China, there are almost 10 tons of vanadium-bearing titanomagnetite concentrates with coexistent titanium and vanadium oxides.[1] As a special and complex iron ore, the vanadium-bearing titanomagnetite mainly consists of ferrous oxides, titanium oxides, vanadium oxides and other oxides such as Al_2O_3, SiO_2, CaO, and MgO.[2] The most common way to utilize vanadium-bearing titanomagnetite concentrates at present is blast furnace iron-making.[3] However, the production of TiC and VC in the smelting process increases the viscosity of slag and thus prevents the separation of slag from hot iron, which is the technical difficulty of the smelting process of vanadium-bearing titanomagnetite concentrates.[4] Moreover, due to some of the vanadium and titanium resources remaining in the slag, high titanium slag is formed, and there is not an appropriate and economic method to deal with such slag yet.[3] Overall, blast furnace iron-making gives rise to an enormous waste of precious resources in the vanadium-bearing titanomagnetite concentrates and brings harm to the environment.[5,6]

In order to make full use of the vanadium-bearing titanomagnetite concentrates, a new application based on its resource characteristics is put forward by our research group, which is the direct preparation of iron-based friction materials by the *in situ* synthesis from vanadium-bearing titanomagnetite concentrates.[7–9]

Since the compositions characteristics of vanadium-bearing titanomagnetite concentrates conform to the composition requirements of iron-based friction material, all the components of this ore are utilized completely. Theoretically, the *in situ* reduction products TiC and VC can be used as reinforced phase of iron-based material owing to their high hardness and good wettability with Fe. Meanwhile, other oxides with high chemical stability such as Al_2O_3, SiO_2, CaO and MgO also contribute to the improved wear-resistance property of iron-based friction materials. As for *in situ* reaction, it has two advantages. On the one hand, the bond strength between reinforcing phases and matrix by *in situ* reaction is higher than that of mechanical mixing. On the other hand, this application is simpler than blast furnace iron-making, and requires lower energy consumption.[10–13]

Our research group previously reported the preparation and properties of an iron-based friction material by *in situ* reaction and sintering in a vacuum from vanadium-bearing titanomagnetite concentrate.[14] The prepared iron-based friction material can merely meet the basic requirement of JBT 3063-1996 but the performance is poor. In order to make further improvements about the performance of the material, an addition of alloying element is considered in this study. The common alloying elements of iron-based material include Cu, Mo, Ni, Mn, which improve properties of iron-based friction material. As the cheapest element among them, Mn and its effects in iron and steel have been given extensive attention.[15–18] This work focuses on effects of Mn on the microstructure and properties of the iron-based friction material by *in situ* carbothermic reaction from

School of Manufacturing Science and Engineering, Sichuan University, Chengdu, 610065, People's Republic of China. E-mail: kqfeng@scu.edu.cn

Table 1 Chemical compositions of vanadium-bearing titanomagnetite concentrates (wt%)

Fe_2O_3	FeO	TiO_2	V_2O_5	Al_2O_3	SiO_2	MgO	CaO	S	P
42.600	30.020	12.650	0.560	4.085	3.890	3.910	1.570	0.677	0.038

vanadium-bearing titanomagnetite concentrates. The findings show that it is promising to find an optimal addition of Mn to greatly improve the tribological properties of the material.

2. Materials and methods

The vanadium-bearing titanomagnetite concentrate powder (≤74 μm) was supplied by Panzhihua Iron and Steel Company (China) and its chemical compositions are shown in Table 1. It indicates that the vanadium-bearing titanomagnetite concentrates are mainly composed of ferrous oxides and titanium oxide. The vanadium-bearing titanomagnetite concentrate powder, Fe powder (≤44 μm, with 99.5% purity), Mn powder (≤44 μm, with 99.5% purity) and graphite (44 μm, with 99.8% purity) which acts as reductant and lubricant are the main materials for the preparation of iron-based friction material. Fe powder, Mn powder and graphite are supplied by Nangong Chunxu Metal Material Co., Ltd.
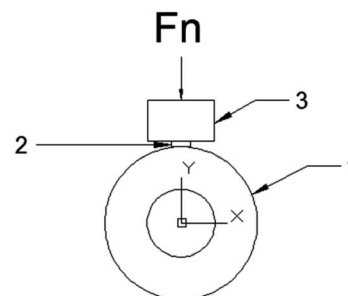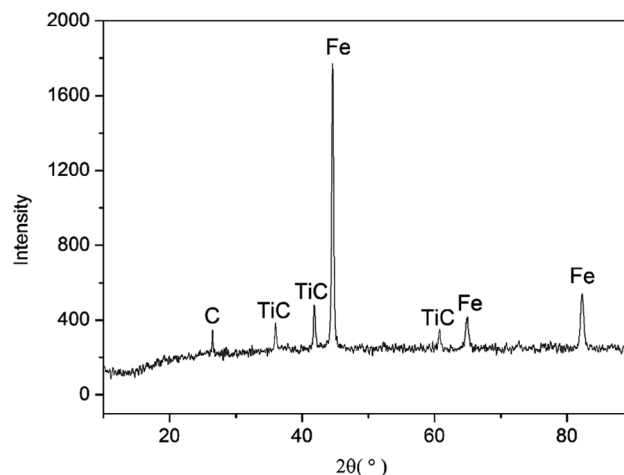
The whole processing route of preparing iron-based friction material from vanadium-bearing titanomagnetite concentrates consists of carbothermic reduction process of vanadium-bearing titanomagnetite concentrates and final sintering process of green samples. In the carbothermic reduction process, the vanadium-bearing titanomagnetite concentrates and reductant graphite (100 wt% : 20.3 wt%) were mixed in the mill at 400 rpm for 4 hours. Then the mixture was heated in the vacuum furnace at 1300 °C for 3 hours. The chemical composition of the obtained pre-reduced powder is listed in Table 2. It can be noted that the vanadium oxides and titanium oxides are respectively converted to VC and TiC. The separate conversion rates of metal iron, TiC and VC from corresponding oxides are about 96%, 75% and 94%.

In the final sintering process, the pre-reduced powder (78.72 wt%), supplementary Fe powder (15.28 wt%) and lubricant graphite powder (6 wt%) were mixed as the basic ingredient according to the composition requirement of typical iron-based friction material. Additionally, the basic ingredient was admixed with different additions of Mn powder (1, 2, 3, 4 wt%). Then the powder mixtures were homogenized in the mill and pressed under 400 MPa by oil hydraulic press machine to obtain green samples, which were named Mn-1, Mn-2, Mn-3, Mn-4, respectively. Besides, the sample without Mn was named Mn-0. Finally, the green samples were sintered in the vacuum of 5 Pa at 1050 °C for 3 hours.

The sintered sample was etched by using 4% nitric acid solution in alcohol for 10 s. The microstructure of sintered

samples was observed with scanning electron microscopy (S-4800). X-ray diffraction (XRD) was used to analyze the phase composition in the sintered samples. The density was tested by Archimedes drainage method. The micro Vickers' hardness and Brinell hardness of sintered samples were measured by HVS-1000 and HBE-3000A, respectively. The chemical states of some typical elements on the worn surfaces were determined using a AXIS UItra DLD X-ray photoelectron spectroscope (XPS).

The schematic illustration of wear test was presented in Fig. 1. The species of dimensions φ 13 mm × 11 mm were conducted on an M-2000 a block-on-ring tester (Zhang Jiakou kehua Testing Machine Manufacturing Co., Ltd). The steel wheel with dimensions φ 36 mm × 10 mm was installed on the fixer. The original weight of the specimens were measured before the test. The rotation speed of the wheel is 210 rpm and the samples were pressed against the wheel with a load of 200 N. After the test, the weight loss was measured by using the precision electron balance model BSA124S (Beijing Sarturius Co., Ltd., China) with the error of 0.1 mg for mass loss determination. Weight loss was converted into volume loss. The

Fig. 1 Diagram of block-on ring tester used in this study. (1). Grinding wheel; (2). specimen; (3). load.

Fig. 2 XRD pattern of the sintered sample of Mn-3.

Table 2 Chemical compositions of pre-reduced powder (wt%)

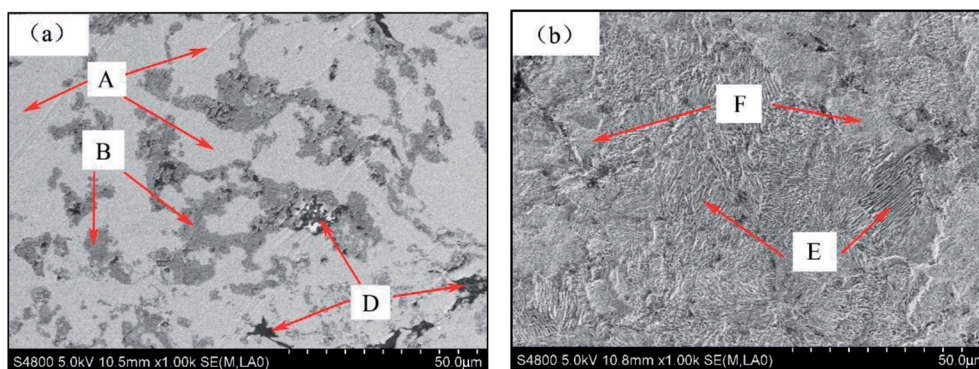| MFe	FeO	TiC	VC	Al_2O_3	SiO_2	MgO	CaO	Others
74.50	1.07	10.69	0.53	5.90	4.71	1.25	1.23	0.13

Fig. 3 Typical microstructure of the unetched (a) and etched (b) sintered sample of Mn-3.

Table 3 EDS analysis results of area A, B, D, E, F. (atom fraction/%)

Area	Fe	C	Ti	V	Mn
A	66.50	31.33	0.68	—	1.49
B	7.43	46.09	44.07	2.00	0.40
D	5.38	94.12	0.14	0.03	0.33
E	74.29	25.71	—	—	—
F	91.98	9.02	—	—	—

coefficient of friction was obtained directly by the M-2000a block-on-ring test. We repeated the wear test of every sintered sample for 3 times.

3. Result and discussion

3.1 The typical phases and microstructure of iron-based friction material

By observing the microstructure of all samples, it can be found that all the microstructure of sintered samples is similar. Since the sintered sample of Mn-3 possesses excellent properties, Mn-3 is selected as the typical sintered sample for discussion as follows. From the X-ray diffraction pattern shown in Fig. 2, it can be seen that main phases are Fe, TiC and C. The SEM micrographs of Mn-3 sintered sample (shown in Fig. 3) show that the microstructure comprises shallow grey region (A), grey region (B) and dark grey region (D). Combined with X-ray diffraction pattern and EDS analysis results listed in Table 3, it is known that the region A (206 HV) is dominated by Fe atoms, Mn atoms which solubilize in Fe atoms and C atoms. Part of C atoms dissolve in Fe atoms and the other part is in the form of Fe_3C. Region B (292 HV) consists of Ti and C atoms, and the ratio of carbon atoms to titanium atoms is near to 1 : 1. Especially, referring to the result of X-ray diffraction pattern, the compound of Ti and C is TiC which acts as hard particles phase. A large amount of C atoms which play a role of lubricant are present in region D (94 HV). Moreover, the iron matrix is composed of Region E and F as shown in Fig. 3(b). Combined with the micro Vickers' hardness of Region E and Region F, it can be indicated that Region E (220 HV) is composed of laminated pearlite and that Region F (162 HV) is comprised of
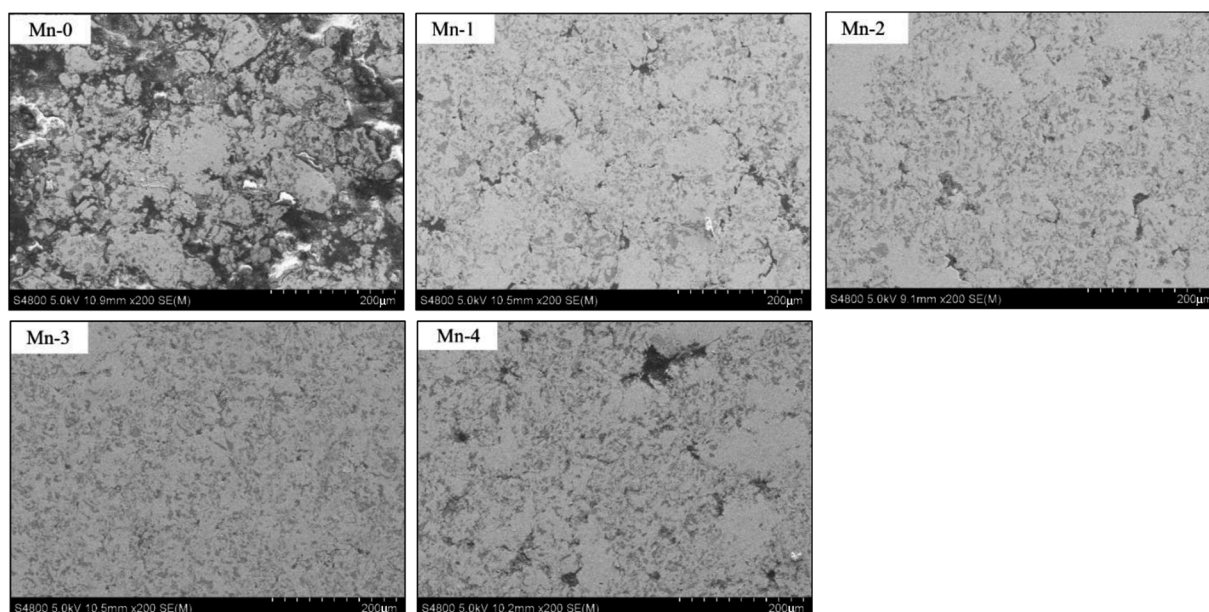

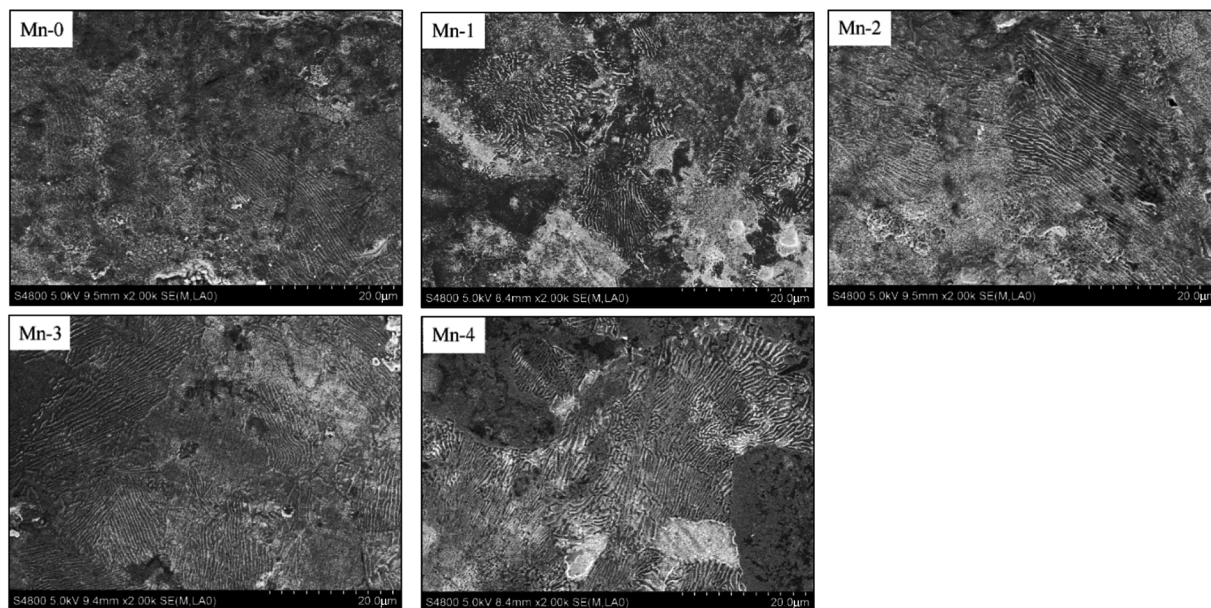**Fig. 4** Microstructure of sintered samples with different Mn contents.

Fig. 5 Laminated pearlite in the etched iron-based friction materials with different Mn contents.

ferrite. Compared with ferrite, the laminated pearlite with thin layers increases the number of phase interface which hinders dislocation motion. As a result, the microstructure with large amount of laminated pearlite contributes to the increasing hardness of iron-based friction material.

3.2 Effect of Mn on the microstructure and properties of iron-based friction material

As shown in Fig. 4, the microstructure of iron-based friction material is improved by Mn element significantly. The matrix of Mn-0 is separated by many uneven pores which are surrounded by agglomerated TiC particles and a great deal of graphite.

When Mn content increases to 3 wt%, the microstructure becomes dense gradually. Not only the number of pores decreases, but also TiC particles and graphite distribute uniformly. When Mn addition exceeds 3 wt%, however the matrix is cut apart by an increasing number of irregular pores, and TiC particles and graphite agglomerate again.

According to evaporation-deposition mechanism of Mn proposed by Šalak A.,[17,18] Mn starts to sublimate at 700 °C. At a sintering temperature of 1050 °C, Mn sublimates remarkably first and then Mn vapor can be homogenized through gas phase transport in the compact. Later, Mn vapor condenses on the surface of iron particles. Since the diffusivity of Mn in Fe is much higher than the self-diffusivity of Fe,[19] Mn diffuses from
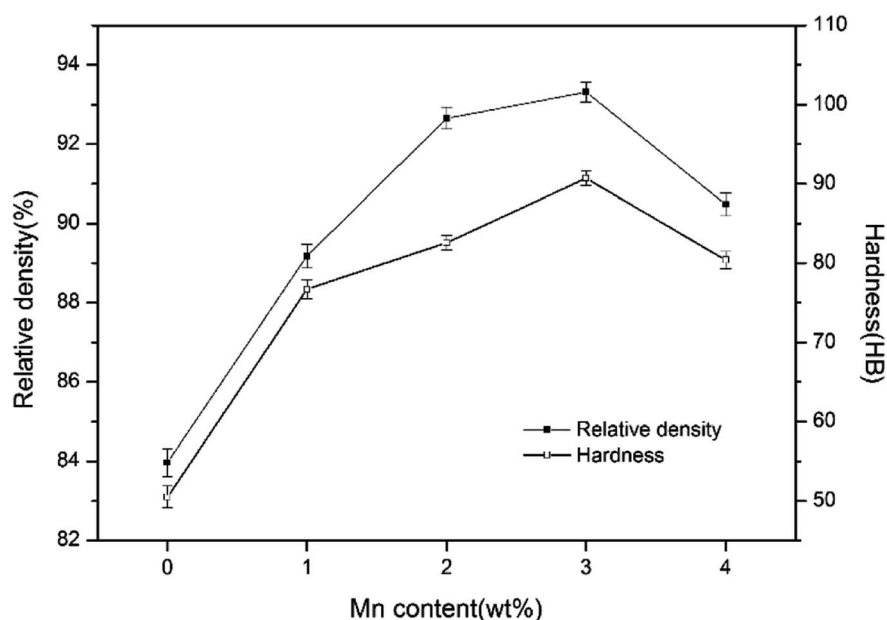

Fig. 6 Effect of Mn addition on hardness and relative density of sintered samples.
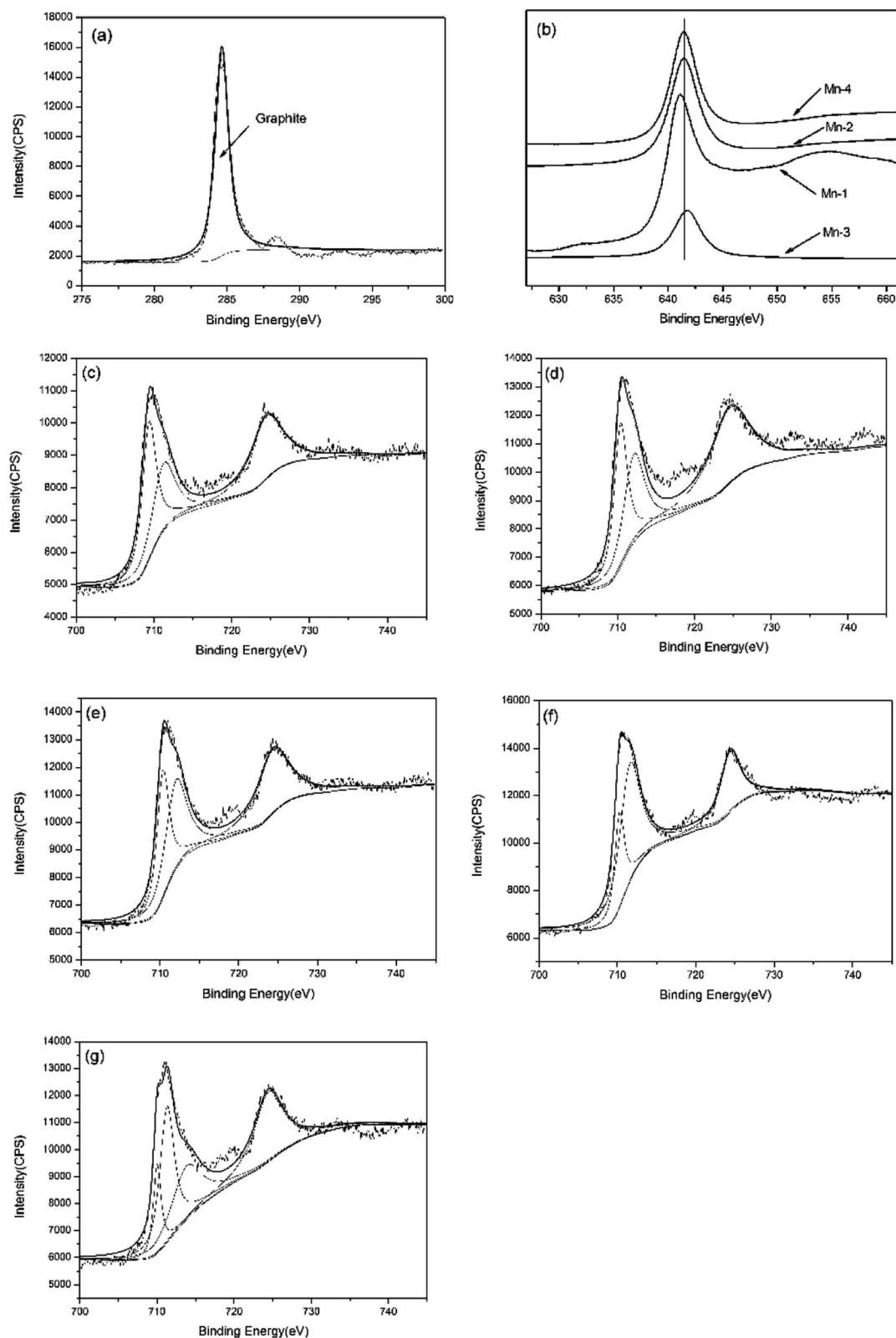
Fig. 7 XPS spectrum of the worn surface of sintered sample with different Mn addition: (a) carbon; (b) manganese; (c) Fe on the worn surface of Mn-0; (d) Fe on the worn surface of Mn-1; (e) Fe on the worn surface of Mn-2; (f) Fe on the worn surface of Mn-3; (g) Fe on the worn surface of Mn-4.

Table 4 Type of the oxides on the worn surface of sintered sample with different Mn addition

Sintered samples	The oxide of Fe	The oxide of Mn
Mn-0	FeO, Fe_2O_3	—
Mn-1	Fe_3O_4, Fe_2O_3	MnO
Mn-2	Fe_3O_4, Fe_2O_3	Mn_2O_3
Mn-3	Fe_3O_4, Fe_2O_3	MnO_2
Mn-4	Fe_3O_4, Fe_2O_3	Mn_2O_3

Table 5 Summary of results on friction coefficient and wear rate of sintered samples

Sintered samples	Friction coefficient	Wear rate ($\times 10^{-7}$ cm^3 J^{-1})
Mn-0	0.540 ± 0.053	1.899 ± 0.21
Mn-1	0.490 ± 0.035	1.309 ± 0.15
Mn-2	0.432 ± 0.021	0.560 ± 0.12
Mn-3	0.400 ± 0.023	0.229 ± 0.07
Mn-4	0.471 ± 0.032	0.424 ± 0.11

the surface to the interior of iron particles gradually, which creates high concentration gradient of vacancy between the surface to the interior of iron particles. Consequently, Fe atoms in the interior of iron particles diffuse to the surface of sintered neck continuously, which promotes the growing of sintered neck. Moreover, since Mn can solute in α-Fe in the form of substitutional atom, the lattice of Fe atom is distorted and the produced the distortional energy facilitates sintering process.[20] As a result, the sintering densification of the material is improved and the spheroidization of pores is promoted.[21,22] However, when Mn exceeds the opportune amount, a great deal of Mn vapor with high partial pressure will enlarge pores,[23] which result in many pores showing in irregular shape in the microstructure.

The characterization of the laminated pearlite in the etched iron-based friction material, shown in Fig. 5, demonstrates that Mn can facilitate the formation of the laminated pearlite. With Mn content increasing, the amount of laminated pearlite rises. Theoretically, since Mn element can expand γ-Fe phase region, with the increase of Mn addition, more and more phase changes from α-Fe to γ-Fe take place and the homogenization of carbon atoms in γ-Fe can be enhanced during the sintering process.[24] Consequently, by means of the decomposition of austenite during the subsequent cooling process, the formation of laminated pearlite can be reinforced.

The relative density and hardness of sintered samples are presented in Fig. 6. It is observed that when Mn content increases to 3 wt%, the relative density rises from 83.97% to 93.32% and hardness increases from 50.5 HB to 90.7 HB. The

change of relative density is directly affected by the sintering densification of sintered samples. The increase of hardness is associated with the higher relative density, an increasing number of laminated pearlite, good solid solution strengthening in Fe and uniform distribution of hard particles.

However, the relative density and hardness value both decrease with further increase of Mn addition. Since a great deal of Mn vapor with high partial pressure enlarges pores in the microstructure, the relative density of samples decreases. The decrease of hardness may be associated with increasing number of irregular pores and agglomerated TiC particles. Consequently, the stress concentration around pores and less effective area to bear external force will bring about the decreasing value of hardness.
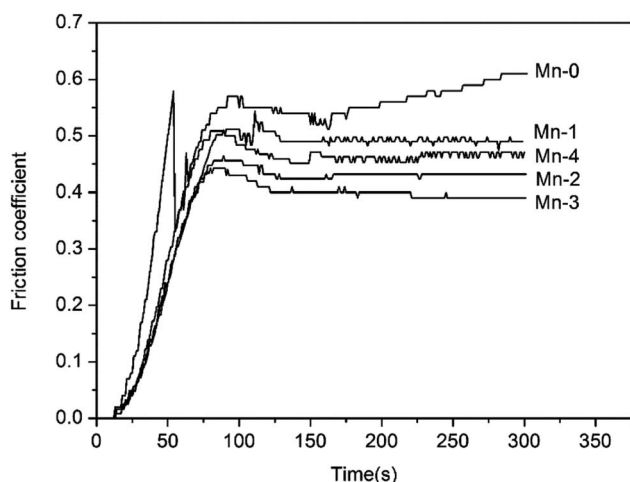
From the above discussions, it can be concluded that 3 wt% Mn addition is most effective to enhance the relative density and hardness of iron-based friction material.

3.3 Effect of Mn on the tribological properties of iron-based friction material

3.3.1 XPS analysis on the worn surface. In order to compare the elements variation of chemical states after sliding, the XPS on Fe, C, Mn are analyzed in detail (shown in Fig. 7) and type of the metal oxides is listed in Table 4. Moreover, the ferrous oxides and manganese oxides are also found on the worn surface.

In the presence of all the sample, the C1s peak can be fitted with the peak with binding energies of 284.8 eV, suggesting that graphite exists on the worn surface.[25] It proves that there is graphite lubricating film on the worn surface. As for Mn-0, the $Fe_{2p3/2}$ peak can be devided into two sub-peaks with binding energies of 709.35 and 711.4 eV, indicating the co-existence of FeO and Fe_2O_3.[25,26] With Mn addition increasing, the ferrous oxide transfers from FeO to Fe_2O_3. Moreover, when the addition of Mn is 1 wt%, the $Mn_{2p3/2}$ peak with 641 eV indicates that MnO exists on the worn surface of Mn-1. With increasing Mn addition, the $Mn_{2p3/2}$ peak of Mn-2 with 641.4 eV and Mn-3 with 641.7 eV mean the existence of Mn_2O_3 and MnO_2, respectively. With further increasing Mn addition, the manganese oxide turns to Mn_2O_3.

3.3.2 The tribological properties of iron-based friction material. The variation of friction coefficient with time of sintered samples with different Mn contents is given in Fig. 8. Summary of results on friction and wear properties of sintered samples are listed in Table 5. As shown in Fig. 8, it can be observed that the friction coefficient of Mn-0 fluctuates severely,

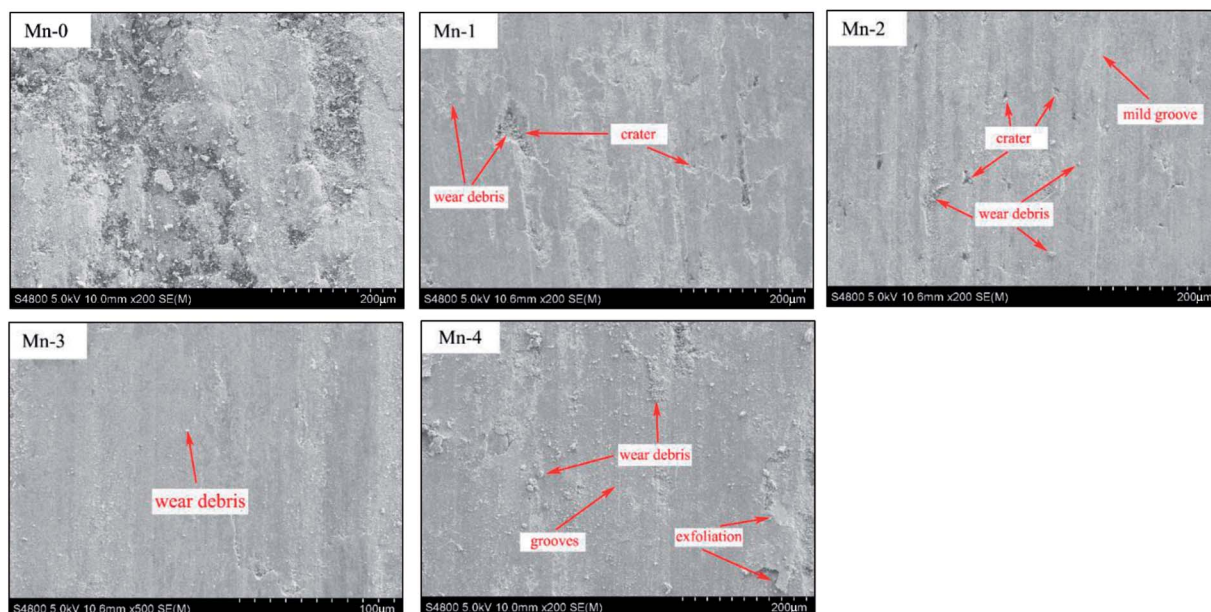**Fig. 8** The variation of friction coefficient of samples with time.

Fig. 9 Worn surface morphologies of sintered samples with different Mn contents.

whereas the curve of friction coefficient of samples with Mn is more stable. Compared with the friction coefficient of Mn-0, the friction coefficient of sintered samples with Mn decreases from 0.54 to 0.40–0.49. From Table 4, when Mn content increases to 3 wt%, the wear rate considerably decreases from 1.899×10^{-7} cm^3 J^{-1} to 0.229×10^{-7} cm^3 J^{-1}. Fig. 9 shows the worn surface morphologies of sintered samples with different Mn contents. The chemical compositions of worn surface of sintered samples are listed in Table 6. It can be noted that all the samples contain significant oxygen contents, which indicates that oxidation occurs on the worn surface during the friction process.

As shown in Fig. 7, wide grooves along the sliding direction, craters, exfoliation and wear debris with 50–100 μm size can be found on the worn surface of Mn-0. During the friction process, the oxide film on the worn surface is formed and it becomes thick and consecutive with friction heat increasing. However, the bearing capacity of the substrate to oxide film is weak owing to its low relative density, thereby, the oxide film exfoliates easily under alternating stress and the fresh iron matrix is exposed. Consequently, the exfoliation of oxides film with high hardness turn to be hard abrasive, which aggravates the wear of Mn-0 and leads to higher wear rate and coefficient.

Combined with chemical compositions of worn surface, it can be noted that the oxygen content on the worn surface of Mn-0 shows a relatively lower value. This may be due to a serious fragmentation and exfoliation of oxides film. In a nutshell, it can be inferred that the wear type is primarily severe abrasive wear, accompanying oxidative wear.

When Mn addition increases from 1 wt% to 3 wt%, not only the number of craters decreases, but also the abrasion grooves become relatively shallower and the worn surface becomes smoother with fine scratches. With the friction process proceeding, the temperature of the friction surface increases and the increasing layers of oxide films are formed in stacks under

pressure continuously. With the increase of the relative density of material, the bearing capacity of the substrate to the oxide film increases. The oxide films protect the surface from being ploughed by the hard abrasive particles, which reduces the possibility of the formation of grooves. Good bearing capacity of the matrix allows the accumulation of oxide films which bear heat, FeO and Mn$_2$O$_3$ were respectively further oxidized to Fe$_2$O$_3$ and MnO$_2$. Therefore, the difference of lattice structure between the oxide film and the effectively restrains the metal bonding and further improves the stability of friction coefficient of the material. Moreover, Hin Jong Han pointed out that the hardness of Fe$_2$O$_3$ is up to 1000 HV.[27] Thus the oxides debris can develop a wear protective layer between the sliding surfaces and avoid direct contact of grinding wheel, which brings about the decrease in wear rate as demonstrated by the results of Fig. 5. As shown in Table 5, when Mn content increases from 1 wt% to 3 wt%, the oxygen content of worn surface increases, which indicates that the oxidative wear is enhanced. Comprehensively, the wear type of material is consisted of mild abrasive wear and oxidative wear.

When Mn addition exceeds 3 wt%, the number of crater increases and oxide film exfoliates, which leads to the decrease of wear rate and friction coefficient. Combined with chemical compositions of worn surface of Mn-4, it can be inferred that the abrasive wear is enhanced.

Table 6 Chemical compositions of worn surface of sintered samples (atom fraction/%)

Sintered samples	C	O	Ti	V	Mn	Fe
Mn-0	29.74	35.90	3.44	0.55	—	30.37
Mn-1	25.27	37.88	2.59	0.46	0.67	33.13
Mn-2	15.59	45.17	1.73	0.39	1.02	36.10
Mn-3	18.29	50.67	1.47	0.20	1.71	27.67
Mn-4	20.37	42.53	1.52	0.40	2.56	32.52

4. Conclusions

In this work, we prepared an iron-based frictional material from vanadium-bearing titanomagnetite concentrates by *in situ* carbothermic reaction with improved tribological properties. The effects of Mn on the microstructures and properties of an iron-based friction material prepared directly from the vanadium-bearing titanomagnetite concentrates, are summarized as follows.

(1). When Mn addition increases to 3 wt%, the sintering densification is enhanced and the amount of laminated pearlites increases. Comparatively, the density and hardness increase rapidly. However, when Mn addition exceeds 3 wt%, pores in the microstructure are enlarged by Mn vapor with high partial pressure, which results in the relative reduction of density and hardness.

(2). With Mn addition increasing from 0 wt% to 3 wt%, tribological properties are improved significantly. The wear rate decreases from 1.899×10^{-7} cm^3 J^{-1} to 0.229×10^{-7} cm^3 J^{-1} and the friction coefficient reduces from 0.54 to 0.40, respectively. However, when Mn addition exceeds 3 wt%, Mn has a negative effect on the tribological properties.

(3). With the increase of Mn, the ferrous oxide changes from FeO to Fe$_2$O$_3$ and manganese oxide transfer from MnO to Mn$_2$O$_3$ and MnO$_2$. The dominant wear mechanism changes from severe abrasive wear to mild abrasive wear and the oxidative wear is enhanced.

Conflicts of interest

The authors declare that they have no conflict of interest.

Acknowledgements

References

1 L. Zhao, Y. Liu, L. Wang, H. Zhao, D. Chen, B. Zhong, J. Wang and T. Qi, Production of Rutile TiO$_2$ Pigment from Titanium Slag Obtained by Hydrochloric Acid Leaching of Vanadium-Bearing Titanomagnetite, *Ind. Eng. Chem. Res.*, 2014, **53**, 70–77.

2 M. Wang, S. Zhou, X. Wang, B. Chen, H. Yang, S. Wang and P. Luo, Recovery of Iron from Chromium Vanadium-Bearing Titanomagnetite Concentrate by Direct Reduction, *JOM*, 2016, **68**, 2698–2703.

3 T. Hu, X. Lv, C. Bai, Z. Lun and G. Qiu, Carbothermic Reduction of Titanomagnetite Concentrates with Ferrosilicon Addition, *ISIJ Int.*, 2013, **53**, 557–563.

4 W. Fu, Y. Wen and H. Xie, Development of Intensified Technologies of Vanadium-Bearing Titanomagnetite Smelting, *J. Iron Steel Res. Int.*, 2011, **18**(7), 18–10.

5 H. Wang, K. Feng, Y. Zhou, Q. Sun and H. Shi, Effects of Na$_2$B$_4$O$_7$·5H$_2$O on the properties of foam glass from waste glass and titania-bearing blast furnace slag, *Mater. Lett.*, 2014, **132**, 176–178.

6 C. Chen, K. Feng, Y. Zhou and H. Zhou, Effect of sintering temperature on the microstructure and properties of foamed glass-ceramics prepared from high-titanium blast furnace slag and waste glass, *Int. J. Miner., Metall. Mater.*, 2017, **24**, 931–936.

7 G. Zhang and K. Feng, Synthesis of iron-based friction material by *in situ* reactive sintering from vanadium-bearing titanomagnetite, *Mater. Manuf. Processes*, 2016, **31**, 198–205.

8 G. Zhang, K. Feng and H. Yue, Theoretical analyses and experimental investigations of selective carbothermal reactions of vanadium-bearing titanomagnetite concentrates for preparation of iron-based wear-resistant material, *JOM*, 2016, **68**, 2525–2532.

9 G. Zhang, K. Feng, Y. Li and H. Yue, Effects of sintering process on preparing iron-based friction material directly from vanadium-bearing titanomagnetite concentrates, *Mater. Des.*, 2015, **86**, 616–620.

10 Y. Bai, S. Cheng and Y. Bai, Analysis of Vanadium-Bearing Titanomagnetite Sintering Process by Dissection of Sintering Bed, *J. Iron Steel Res. Int.*, 2011, **18**(6), 8–15.

11 Y. Lei, J. Jiang, T. Bi, J. Du and X. Pang, Tribological behavior of in situ fabricated grapheme-nickel matrix composites, *RSC Adv.*, 2018, **8**, 22113–22121.

12 R. Khoshhal, M. Soltanieh and M. A. Boutorabi, Formation mechanism and synthesis of Fe-TiC/Al$_2$O$_3$ composite by ilmenite, aluminum and graphite, *Int. J. Refract. Met. Hard Mater.*, 2014, **45**, 53–57.

13 D. Yang, Y. Liu, H. Ding, J. Chen, Z. Huang and D. Ye, Synthesis of β- sialon/Ti(C, N) powders from mineral waste residue *via* carbothermic reduction nitridation, *RSC Adv.*, 2014, **4**, 31493–31502.

14 H. Yue, K. Feng, Y. Li and G. M. Zhang, Effect of graphite content on Fe-based friction material prepared by *in situ* carbothermic reduction and synthesis from vanadium and titanium iron concentrate, *Trans. Mater. Heat Treat.*, 2015, **36**, 16–21.

15 L. Li, W. Yang and Z. Sun, Influence of Mn content on dynamic recrystallization of ferrite in low carbon steels, *Acta Metall. Sin.*, 2004, **40**, 1257–1263.

16 W. D. Callister, *Fundamentals of Materials Science and Engineering: An Integrated Approach*, 2nd edn, John Wiley and Sons Ltd, 2005.

17 A. Šalak, Manganese sublimation and carbon ferromanganese liquid phase formation during sintering of premixed manganese steels, *Int. J. Powder Metall. Powder Technol.*, 1980, **16**, 369–397.

18 A. Šalak, Sintered manganese steels (part II): manganese evaporation during sintering, *Powder Metall. Int.*, 1980, **12**, 72–75.

19 J. Smithells, *ColinSmithells metals reference book*, Butterworth-Heinemann, 1983.

20 J. Ruan and P. Huang, *Principle of powder metallurgy*, China machine press, 2012.

21 A. Šalak, Manganese vapor-protection of premixed manganese steels against oxidation during sintering, *Powder Metall. Int.*, 1986, **18**, 267–270.

22 Z. Li, M. Zhao, S. Luo and J. Yi, High strength low-alloy sintered steel containing manganese(II)—Adding strategies and characteristics of sintering process, *Materials Science and Engineering of Powder Metallurgy*, 2008, **13**, 125–131.

23 L. Hu, Z. Xiao, W. Fu, Y. Lu, L. Chen and D. Ni, Effect of manganese content on microstructure and properties of Fe-Cu-Mn-C sintering alloy, *Materials Science and Engineering of Powder Metallurgy*, 2013, **18**, 821–826.

24 M. M. Aranda, B. Kim, R. Rementeria, C. Capdevila and C. G. D. Andrés, Effect of Prior Austenite Grain Size on Pearlite Transformation in a Hypoeuctectoid Fe-C-Mn Steel, *Mater. Sci. Eng., A*, 2014, **45**, 1778–1786.

25 C. D. Wagner, *Handbook of X-ray Photoelectron Spectroscopy*, Perkin-Elmer, Physical Electronic Division, MI, 1979.

26 Y. Chen, X. H. Li and P. L. Wu, Enhancement of structural stability of nanosized amorphous Fe_2O_3 powders by surface modification, *Mater. Lett.*, 2007, **61**, 1223–1226.

27 J. H. Shin, D. S. Lim and H. S. Ahn, Effect of annealing and Fe_2O_3, addition on the high temperature tribological behavior of the plasma sprayed yttria-stabilized zirconia coating, *Surf. Coat. Technol.*, 2000, **133**, 403–410.